REGULAR PAPER

Flux balance analysis of *Chlorella* sp. FC2 IITG under photoautotrophic and heterotrophic growth conditions

Muthusivaramapandian Muthuraj · Basavaraj Palabhanvi · Shamik Misra · Vikram Kumar · Kumaran Sivalingavasu · Debasish Das

Abstract Quantification of carbon flux distribution in the metabolic network of microalgae remains important to understand the complex interplay between energy metabolism, carbon fixation, and assimilation pathways. This is even more relevant with respect to cyclic metabolism of microalgae under light–dark cycle. In the present study, flux balance analysis (FBA) was carried out for an indigenous isolate *Chlorella* sp. FC2 IITG under photoautotrophic and heterotrophic growth conditions. A shift in intracellular flux distribution was predicted during transition from nutrient sufficient phase to nutrient starvation phase of growth. Further, dynamic flux analysis (dFBA) was carried out to capture light–dark metabolism over discretized pseudo steady state time intervals. Our key findings include the following: (i) unlike heterotrophic condition, oxidative pentose phosphate (PP) pathway, and Krebs cycle were relatively inactive under photoautotrophic growth; (ii) in both growth conditions, while transhydrogenation reaction was highly active, glyoxalate shunt was found to be nonoperative; (iii) flux distribution during transition period was marked with up regulation of carbon flux toward nongrowth associated (NGA) maintenance energy, oxidative phosphorylation, and photophosphorylation; (iv) redirection of carbon flux from polysaccharide and neutral lipid resulted in up regulation of Krebs cycle flux in the dark phase; (v) elevated glycolytic and acetyl-CoA flux were coupled with induction of neutral lipid during light cycle of the growth; (vi) significantly active photophosphorylation in the light phase was able to satisfy cellular energy requirement without need of oxidative PP pathway; and (vi) unlike static FBA, dFBA predicted an unaltered NGA maintenance energy of 1.5 mmol g^{-1} DCW h^{-1}.

List of symbols

v_{PS}^{kin}	Flux of polysaccharide metabolism obtained from kinetic model (mmol g^{-1} h^{-1})
v_{PS}^{fba}	Flux of polysaccharide metabolism obtained from FBA (mmol g^{-1} h^{-1})
v_{Prt}^{kin}	Flux of protein metabolism obtained from kinetic model (mmol g^{-1} h^{-1})
v_{Prt}^{fba}	Flux of protein metabolism obtained from FBA (mmol g^{-1} h^{-1})
v_{NL}^{kin}	Flux of neutral lipid metabolism obtained from kinetic model (mmol g^{-1} h^{-1})
v_{NL}^{fba}	Flux of neutral lipid metabolism obtained from FBA (mmol g^{-1} h^{-1})
v_{PL}^{kin}	Flux of phospholipid metabolism obtained from kinetic model (mmol g^{-1} h^{-1})
v_{PL}^{fba}	Flux of phospholipid metabolism obtained from FBA (mmol g^{-1} h^{-1})

Muthusivaramapandian Muthuraj and Basavaraj Palabhanvi have contributed equally to this study.

M. Muthuraj · B. Palabhanvi · K. Sivalingavasu · D. Das (✉)
Department of Biotechnology, Indian Institute of Technology Guwahati, Guwahati 781039, Assam, India
e-mail: debasishd@iitg.ernet.in; debasis.iitb@gmail.com

S. Misra · V. Kumar · D. Das
Centre for Energy, Indian Institute of Technology Guwahati, Guwahati 781039, Assam, India

v_{DNA}^{kin} Flux of DNA metabolism obtained from kinetic model (mmol g^{-1} h^{-1})

v_{DNA}^{fba} Flux of DNA metabolism obtained from FBA (mmol g^{-1} h^{-1})

v_{RNA}^{kin} Flux of RNA metabolism obtained from kinetic model (mmol g^{-1} h^{-1})

v_{RNA}^{fba} Flux of RNA metabolism obtained from FBA (mmol g^{-1} h^{-1})

v_{Chl}^{kin} Flux of chlorophyll metabolism obtained from kinetic model (mmol g^{-1} h^{-1})

v_{Chl}^{fba} Flux of chlorophyll metabolism obtained from FBA (mmol g^{-1} h^{-1})

Introduction

Photosynthetic microorganisms e.g., microalgae and cyanobacteria have been used for various applications such as waste water treatment, single cell protein synthesis for human, and animal consumption and as potential source for various value added products (Rodolfi et al. 2009). These applications are based on photoautotrophic metabolism, which utilizes solar radiation as a source of energy and photosynthetic machinery to convert inorganic carbon into diverse organic matters to satisfy the requirements of microorganism. Some of these photosynthetic organisms could be renewable sources of biodiesel as they accumulate significant amount of lipid in their biomass (Hu et al. 2008). Microalgal biodiesel has gained significant interest as these unicellular photosynthetic organisms possess faster growth rate and produce more oil per unit area than plant (Hu et al. 2008). Therefore, efficient utilization of microalgae as cell factory for biodiesel production is linked to complete understanding of interaction between energy metabolism, carbon fixation and assimilation pathways.

Quantification of carbon flux distribution in the metabolic network of various organisms has been found important to understand the complex interplay between genotypic alterations and the corresponding phenotypic response (Shastri and Morgan 2005; Boyle and Morgan 2009). Estimation of carbon flux distribution via flux balance analysis (FBA) relies on pseudo steady state approximation, and hence, no information on metabolite concentrations or time evolution of flux values can be obtained from this analysis (Varma and Palsson 1994). Dynamic flux analysis (dFBA) on the other hand has the ability to predict the dynamic characteristics of flux distribution during the transition between two steady states by incorporating the rate of change in flux constraints (Mahadevan et al. 2002). In a photosynthetic organism like microalgae cellular metabolism may occur in cyclic fashion due to change in environmental cues like light–dark cycle. This cyclic metabolism may cause changes in

intracellular composition of the biomass over light–dark period. While pseudo steady state assumption may be applicable over exponential phase of the growth, dynamic changes in the cellular composition, and in turn flux distributions during light and dark cycle can be modeled more accurately using dFBA. In recent reports, dynamic FBA was employed to capture change in flux distribution during diauxic growth of *Escherichia coli* (Mahadevan et al. 2002) and plant carbohydrate metabolism (Kleessen and Nikoloski 2012). To our knowledge, no such dFBA has been carried out to capture cyclic metabolism of microalgae under light–dark cycle.

In the present study, FBA was carried out for a novel isolate *Chlorella* sp. FC2 IITG (hereafter referred as FC2) under photoautotrophic and heterotrophic growth conditions. While the strain exhibited biomass titer in the lower range (0.7–1.0 g L^{-1}), the neutral lipid content was higher (37.64–59.69 %, w/w DCW) as compared to the other strains reported in the literature (Lim et al. 2012). Therefore, the strain FC2 could be a suitable candidate for biodiesel production. The analysis was based on the development of stoichiometric model for the organism coupled with linear programming optimization. While extracellular nutrient uptake rates were used as the model inputs, validation of the metabolic model was performed by comparing model predicted specific growth rate or carbon flux toward formation of neutral lipid with the corresponding experimental values. Further, a shift in intracellular flux distribution was predicted during transition from nutrient sufficient phase to nutrient starvation phase. While the nutrient sufficient phase is marked with phosphate sufficient condition in the medium, the nutrient starvation phase corresponds to phosphate exhausted condition. Finally, dFBA was employed to capture time evolution of carbon flux distribution during light–dark cycle via integration of kinetic model with FBA. These results point toward possible regulation of lipid biosynthesis in FC2 and in turn rate limiting steps which could be potential targets for metabolic engineering.

Materials and methods

Organism, bioreactor and cultivation condition

FBA was performed for an indigenous microalgal strain FC2 (Accession Number: JX154075) which was isolated from freshwater of Indian Institute of Technology, Guwahati, Assam, India. The strain FC2 was characterized under photoautotrophic and heterotrophic cultivation conditions in a 3.0 L automated bioreactor (Bio Console ADI 1025, Applikon Biotechnology, Holland) with BG11 medium, at 28 °C, pH 7–8, and aeration at 1 vvm. Under photoautotrophic cultivation, the cells were grown with 1 % (v/v) CO_2,

and light intensity of 20 μmol photons m^{-2} s^{-1} for a light:dark cycle of 16:8 h. Under heterotrophic condition, BG11 medium was supplemented with initial glucose concentration of 15 g L^{-1} as the sole energy and carbon source in dark. These experimental data used in the FBA were obtained from unpublished study carried out in our laboratory. In order to validate dFBA model, the culture was further grown under same conditions as mentioned above for the photoautotrophic growth with enhanced light intensity of 35 μmol photons m^{-2} s^{-1} for a light: dark cycle of 16:8 h. To capture the changes in macromolecular composition of the biomass, a frequent sampling strategy was adopted for two light cycles (48–64 and 72–88 h) and two dark cycles (64–72 and 88–96 h) over the time period of 48–96 h: (in hours after light on) 0.5, 4.5, 8.5, 12.5, 15.5 and (in hours after light off) 0.5, 4.5, 7.5. Dynamic profiles of utilization of nitrate (Cataldo et al. 1975), phosphate (Parsons et al. 1984), growth, and intracellular biomass composition such as protein (Pruvost et al. 2011), carbohydrate (Pruvost et al. 2011), neutral lipid, (Chen et al. 2009) and chlorophyll fraction (Pruvost et al. 2011) were measured at every sampling time points.

Flux balance analysis

FBA was performed based on three key steps: defining the biological system via reconstruction of metabolic network, formulation of reconstructed metabolic network into a stoichiometric model, and solving stoichiometric model using linear programming with a suitable objective function (Shastri and Morgan 2005). In the present study, the metabolic network for FC2 was reconstructed from the gene–protein-reaction associations for green algae *Chlamydomonas reinhardtii* available in KEGG database (Kanehisa et al. 2008) and other relevant literatures (Shastri and Morgan 2005; Boyle and Morgan 2009; DalMolin et al. 2011). All the reactions (detailed list is given in the Online Resource S1) were elementally balanced except for protons (Montagud et al. 2010) and water molecules. The FBA model captures cellular behavior under pseudo steady state conditions, where the metabolic model is transformed to a stoichiometric model $S \cdot v = 0$, S is the stoichiometric matrix that contains the stoichiometric coefficients of i metabolites in the j reactions, and v is the flux vector that corresponds to the flux of the j reactions (Srivastava et al. 2012). Dimensions of the stoichiometric matrices were 114×161 and 113×158 for photoautotrophic and heterotrophic growth, respectively, where rows represent metabolites and columns represent reactions. Finally, the stoichiometric model was solved using linear programming by defining a suitable objective function. Changes in the flux distribution during transition from nutrient sufficient phase to nutrient starvation phase were captured via flux

analysis at 72 and 96 h of cultivation, respectively. It is important to note that both nutrient sufficient phase and nutrient starvation phase fall in the exponential phase of growth (Fig. 1 in Online Resource S2). *Maximization of biomass* (M_μ) was used as the objective function for flux analysis at 72 h time point. Whereas, flux estimation at 96 h time point was performed using two different objective functions: (i) *maximization of biomass* and (ii) *maximization of neutral lipid* (M_{NL}). The rationale behind considering two different objective functions for FBA at 96 h time point were to test the suitability of M_μ as objective function at that time point, when the cells were experiencing a shift in growth environment in terms of transition from nutrient sufficient phase to the nutrient starvation phase and likely to maximize accumulation of neutral lipid. Therefore, the flux estimates obtained from FBA using M_μ was compared with the corresponding values obtained from flux analysis using M_{NL} at 96 h time point. For photoautotrophic growth the model inputs were experimentally determined uptake rates for nitrate, photon flux, and carbon dioxide, whereas for heterotrophic growth glucose and nitrate uptake rates were used as the model inputs. In case of objective function M_{NL}, experimentally obtained specific growth rate was also used as the model input along with the above mentioned inputs. FBA was performed by *fmincon* routine in MATLAB (MATHWORK, Natick, MA) which uses linear programming based optimization algorithm.

Dynamic Flux balance analysis (dFBA)

In the dFBA, kinetic model was coupled with steady state FBA (Mahadevan et al. 2002; Yugi et al. 2005) to capture the dynamic flux distribution during light–dark cycles over the time period of 48–96 h in the exponential growth phase of FC2 under photoautotrophic cultivation. A schematic representation of dFBA employed in the present study is shown in Fig. 1. Dynamic FBA involves following steps: (i) development of kinetic model to predict dynamic profile of substrate (nitrate, phosphate, dissolved CO_2) utilization, growth, and changes in intracellular biomass composition (protein, carbohydrate, and neutral lipid); (ii) estimation of kinetic parameters by fitting simulated dynamic profile of substrates, biomass, and intracellular compositions with the corresponding experimental values followed by model validation; and (iii) incorporation of the dynamic reaction rates (fluxes) predicted by kinetic model as inputs for FBA. The entire time period from 48 to 96 h of cultivation was divided into 48 pseudo steady state time intervals of 1 h each. The FBA was performed for each time interval with uptake rates for nitrate, phosphate, photon flux, and carbon dioxide as the model inputs which undergo instantaneous transition between two adjacent pseudo steady state
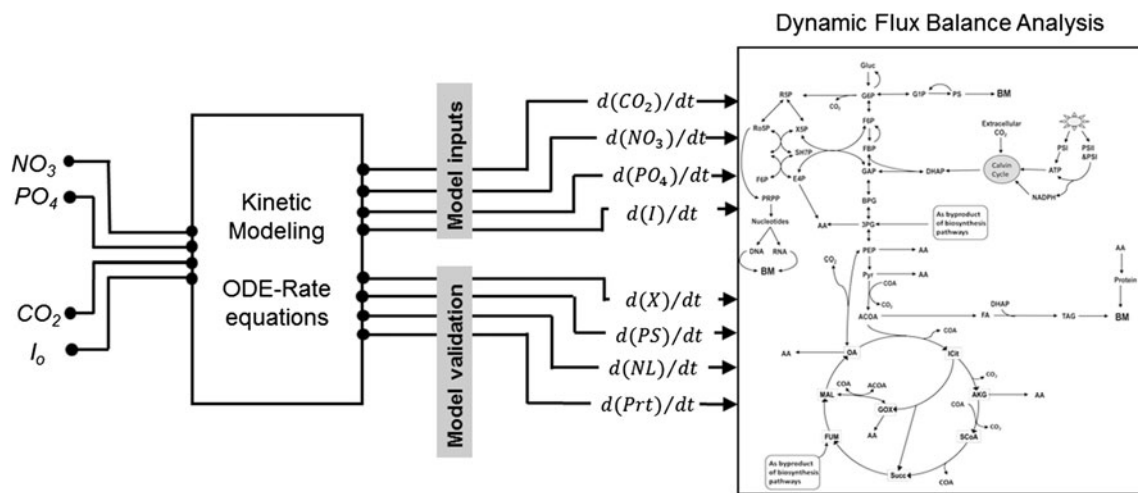
Fig. 1 Schematic representation of the steps involved in the dFBA. The dFBA consist of three steps: (i) development of kinetic model to predict dynamic profile of substrates, growth, and intracellular biomass composition; (ii) estimation of kinetic parameters by fitting simulated dynamic profiles with the corresponding experimental values; and (iii) integrating dynamic reaction rates (fluxes) predicted by kinetic model as inputs for dFBA

intervals. The objective function was minimization of error between FBA predicted flux for intracellular components and corresponding values predicted by the kinetic model:

$$
\begin{aligned}
\mathrm{Obj} = \min \Bigg[& \left(\frac{v_{\mathrm{PS}}^{\mathrm{kin}} - v_{\mathrm{PS}}^{\mathrm{fba}}}{v_{\mathrm{PS}}^{\mathrm{kin}}} \right)^2 + \left(\frac{v_{\mathrm{Prt}}^{\mathrm{kin}} - v_{\mathrm{Prt}}^{\mathrm{fba}}}{v_{\mathrm{Prt}}^{\mathrm{kin}}} \right)^2 + \left(\frac{v_{\mathrm{NL}}^{\mathrm{kin}} - v_{\mathrm{NL}}^{\mathrm{fba}}}{v_{\mathrm{NL}}^{\mathrm{kin}}} \right)^2 \\
& + \left(\frac{v_{\mathrm{PL}}^{\mathrm{kin}} - v_{\mathrm{PL}}^{\mathrm{fba}}}{v_{\mathrm{PL}}^{\mathrm{kin}}} \right)^2 + \left(\frac{v_{\mathrm{DNA}}^{\mathrm{kin}} - v_{\mathrm{DNA}}^{\mathrm{fba}}}{v_{\mathrm{DNA}}^{\mathrm{kin}}} \right)^2 \\
& + \left(\frac{v_{\mathrm{RNA}}^{\mathrm{kin}} - v_{\mathrm{RNA}}^{\mathrm{fba}}}{v_{\mathrm{RNA}}^{\mathrm{kin}}} \right)^2 + \left(\frac{v_{\mathrm{Chl}}^{\mathrm{kin}} - v_{\mathrm{Chl}}^{\mathrm{fba}}}{v_{\mathrm{Chl}}^{\mathrm{kin}}} \right)^2 \Bigg]
\end{aligned} \tag{1}
$$

The details on model development and parameter estimation is given in the Online Resource S2.

Biomass composition

Analysis of elemental composition (in weight fractions) of dry biomass was found to constitute as follows: 53.44 % carbon, 7.71 % hydrogen, 6.62 % nitrogen, and 32.23 % oxygen for photoautotrophic condition; and 56.58 % carbon, 8.49 % hydrogen, 3.54 % nitrogen, and 31.39 % oxygen for heterotrophic condition. Analysis of macromolecular composition of the biomass includes carbohydrate, protein, chlorophyll, and neutral lipid content. In case of FBA the ratio of RNA to DNA was assumed to be 28 (Boyle and Morgan 2009), and RNA content in the biomass was assumed to be a constant (2.8 % of dry biomass) in all conditions of growth (Yang et al. 2000; Fuentes et al. 2000). A constant nucleic acid fraction of 1 % of dry biomass was assumed for dFBA analysis. The polar lipid composition in the biomass was as follows: 50 % Mono-galactosyl diacylglycerol, 20 % Di-galactosyl diacylglycerol, 10 % Sulfoquinovosyl diacylglycerol, 10 % Phosphatidyl glycerol, 5 % Phosphatidyl ethanolamine, and 5 % Phosphatidyl inositol (El-sheekh 1993; Dormann and Benning 2002). The composition of total fatty acid of the biomass was obtained by gas chromatography analysis. Based on the analysis and assumptions, a different biomass equation was formulated for different cultivation conditions and for different phases (nutrient sufficient phase and nutrient starvation phase) of a specific cultivation condition (Table 1).

Measureable external fluxes

Additional constraints such as maximum nutrient uptake rate and product formation rates are essential to simulate growth of the organism. Under photoautotrophic growth, CO_2 consumption rate (v_{co_2}) was obtained from cellular carbon content (x), and specific growth rate (μ) of the organism and was calculated using the formula $v_{co_2} = \left(\frac{x}{12} \right) \mu$. The presence of any other overflow products as potential sink for carbon assimilation was assumed to be negligible. A photon flux of 13.5 and 83.5 mmol g^{-1} DCW h^{-1} was used as the lower and upper bound which corresponds to the nutrient starvation phase and nutrient sufficient phase of the growth, respectively. Whereas in case of dFBA, the photon flux was varied from 18.5 mmol g^{-1} DCW h^{-1} (at 96 h) to 101 mmol g^{-1} DCW h^{-1} (at 48 h). Growth associated (GA) and nongrowth associated (NGA) maintenance energy utilizations were considered in the metabolic model which accounts for growth and survival of the organism, respectively. GA maintenance energy requirement was assumed to be 39.24 mmol ATP g^{-1} DCW for photoautotrophic condition, and 38.78 mmol ATP g^{-1} DCW for heterotrophic condition

Table 1 Experimentally determined biomass composition for *Chlorella* sp. FC2 IITG under photoautotrophic and heterotrophic cultivation conditions at nutrient sufficient (72 h) and nutrient starvation (96 h) phase

Metabolites	Biomass composition, % (w/w)				Reference
	Photoautotrophic cultivation		Heterotrophic cultivation		
	72 h	96 h	72 h	96 h	
Neutral lipid	1	9.97	12.9	29.97	Experimentally determined
Polar lipid	9.59	9.1	8.3	7.91	Determined by equating the components to 100 %
Polysaccharide	52.99	57.3	42.36	29.62	Experimentally determined
Protein	29.3	17.77	32.04	28.12	Experimentally determined
DNA	0.1	0.1	0.1	0.1	Boyle and Morgan (2009)
RNA	2.8	2.8	2.8	2.8	Yang et al. (2000) and Fuentes et al. (2000)
Chlorophyll	4.13	2.98	1.5	1.48	Experimentally determined

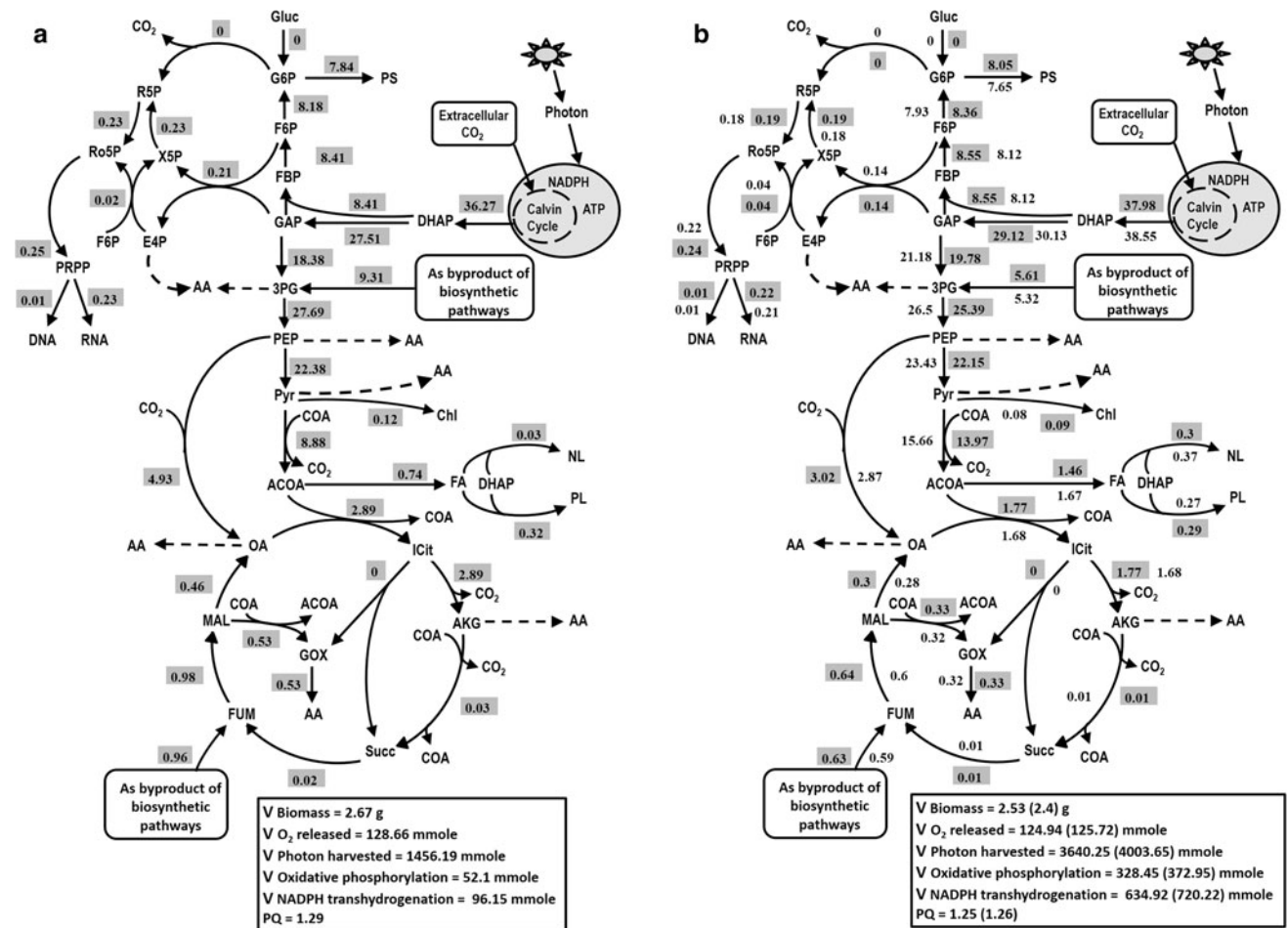The values represent the % (w/w) of dry biomass

Fig. 2 Distribution of carbon fluxes under photoautotrophic cultivation **a** at 72 h with maximization of biomass as objective function and **b** at 96 h with two different objective functions *maximization of biomass* (flux values are shown in *shaded box*) and *maximization of neutral lipid* (flux values are shown *without box*). All the flux values are normalized to 100 mmol CO_2 assimilated and are measured in mmol g^{-1} DCW h^{-1}

which is same as that reported for *Chlamydomonas reinhardtii* (Boyle and Morgan 2009). NGA maintenance energy was obtained by fitting the model to experimentally determined fluxes for growth.

Results and discussion

Flux distribution under heterotrophic and photoautotrophic growth of FC2

Photoautotrophic and heterotrophic growths were simulated using reconstructed metabolic network to calculate the intracellular carbon fluxes of FC2 at 72 h of growth (Figs. 2a, 3a). Comparison of model predicted and experimentally determined specific growth rates exhibited a similarity of 93 and 98 % for photoautotrophic and heterotrophic growth

conditions, respectively (Table 2). Under heterotrophic growth, the flux distribution in central metabolic pathways started with glucose uptake and, 50 % of the total carbon influx was directed toward glycolysis pathway (Fig. 3a) at glucose-6-phosphate (G6P) node. The second major fraction of the incoming carbon flux was channeled into pentose phosphate (PP) pathway (32 %) followed by distribution of the remaining flux toward polysaccharide biosynthesis, which was attributed toward synthesis of cell wall components and storage carbohydrates (Barsanti and Gualtieri 2006). C^{13} based analyses in *Chlorella protothecoides* showed similar flux bifurcations at the G6P node (glycolysis—54.4 % and PP pathway—33.3 %) under heterotrophic condition (Xiong et al. 2010). The majority of this carbon flux partitioning between glycolysis and PP pathway at the G6P node provides large amount of biosynthetic precursors, chemical energy, and reducing equivalent required for active cellular metabolism.
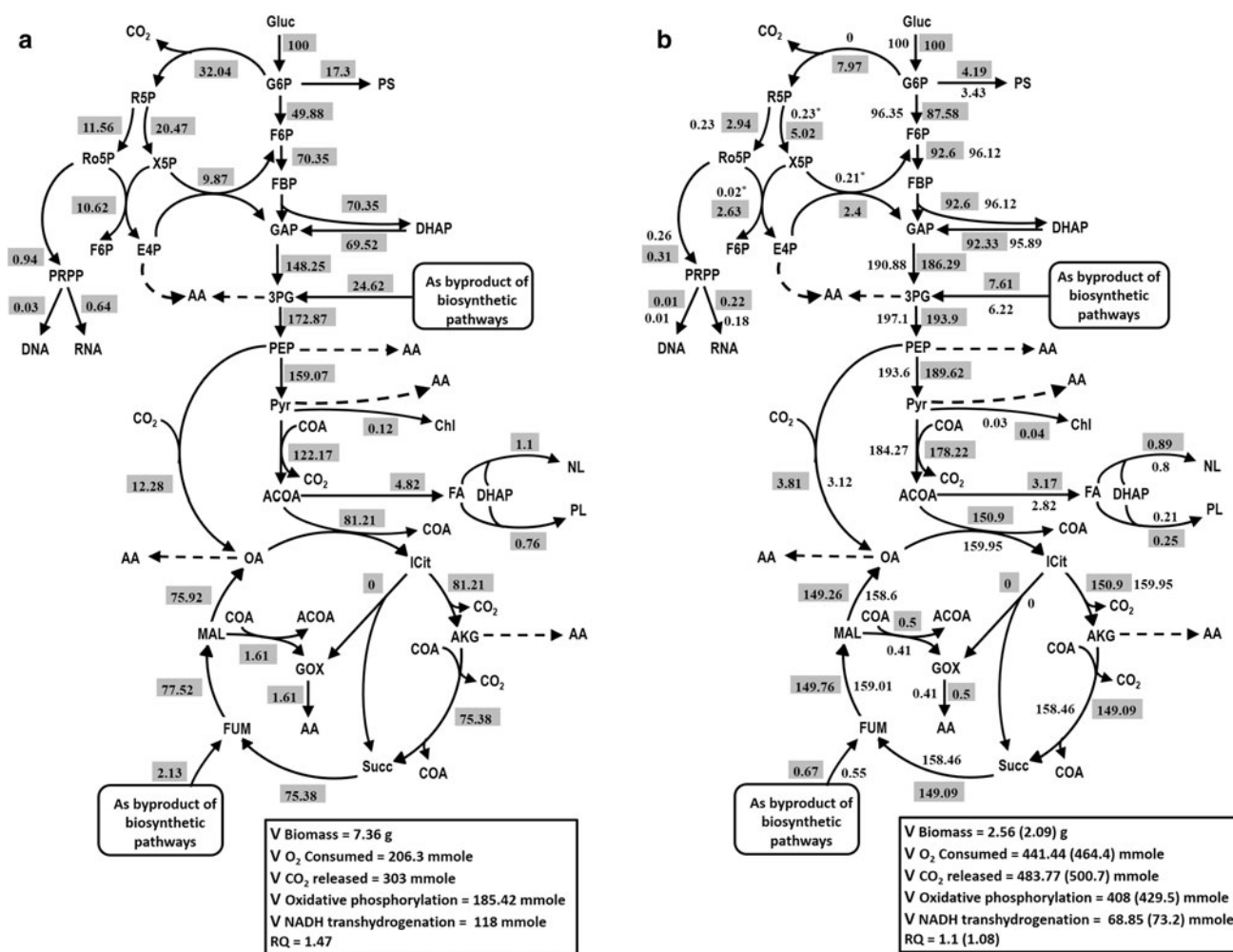

Fig. 3 Distribution of carbon fluxes under heterotrophic cultivation **a** at 72 h with maximization of biomass as objective function and **b** at 96 h with two different objective functions *maximization of biomass* (flux values are shown in *shaded box*) and *maximization of neutral lipid* (flux values are shown *without box*). All the flux values are normalized to 100 mmol glucose assimilated and are measured in mmol g^{-1} DCW h^{-1}. '*' represents the flux opposite to the direction of the *arrow*

Table 2 Comparison of model predicted and experimentally determined specific growth rates (h^{-1}) and neutral lipid flux (mmol g^{-1} h^{-1}) under photoautotrophic and heterotrophic growth conditions

Growth condition	Specific growth rate μ (h^{-1})[a]				Neutral Lipid flux (mmol g^{-1} h^{-1})[b]	
	72 h		96 h		96 h	
	Experimental	Predicted	Experimental	Predicted	Experimental	Predicted
Photoautotrophic	0.045	0.048	0.031	0.035	0.0046	0.00483
Heterotrophic	0.054	0.055	0.031	0.038	0.0115	0.0119

[a] Objective function *maximization of biomass* was used for the flux analysis at 72 and 96 h of growth

[b] Objective function *maximization of neutral lipids* was used for the flux analysis at 96 h of growth
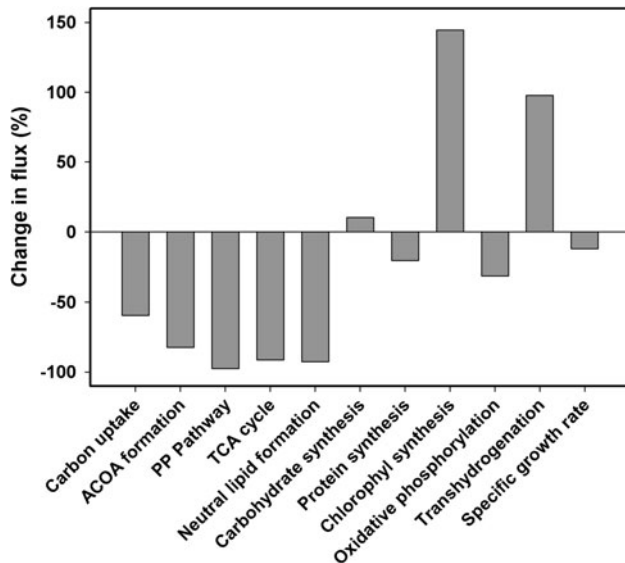

Fig. 4 Percentage change in absolute flux values under photoautotrophic condition with respect to heterotrophic condition at 72 h of growth. Heterotrophic fluxes were normalized with respect to C-mole basis while comparing with photoautotrophic flux values

Under photoautotrophic condition the carbon flux distribution started with Calvin cycle by fixing CO_2 in the form of 3-phosphoglycerate (3PG) which gets further converted to dihydroxy acetone phosphate (DHAP). A part of this DHAP carbon flux was bifurcated toward gluconeogenesis pathway (46.37 %) leading to the formation of polysaccharides, and the remaining fraction flowed through glycolytic pathway (Fig. 2a). Similar flux distribution in the DHAP node was observed in case of *C. pyrenoidosa* cultivated under photoautotrophic condition with maximum carbon flux bifurcating to the glycolytic pathway (Yang et al. 2000). Flux through PP pathway and TCA cycle under photoautotrophic condition was found to be 97.45 and 91.37 % lesser than heterotrophic condition, respectively (Fig. 4). While these low TCA cycle and PP pathway fluxes may be sufficient to provide precursors for biosynthetic pathways, the requirements for ATP and reducing power were fulfilled through photophosphorylation in the light harvesting photosystems I and II (Yang et al. 2000; Shastri and Morgan 2005).

Under heterotrophic metabolism, 27.07 and 8.19 % of initial carbon uptake flux from Acetyl-CoA (ACOA) node and anapleurotic reaction (Phosphoenol pyruvate (PEP) carboxylase), respectively was streamed through TCA cycle. However, majority of this carbon flux was lost in the form of CO_2 for energy production as also reported in the literature (Shastri and Morgan 2005). A relatively higher anapleurotic carbon uptake flux (19.72 %) was observed in case of photoautotrophic condition. Existence of this active anapleurotic pathway points toward its role in replenishing oxaloacetate in TCA cycle under inactive glyoxylate shunt (Xiong et al. 2010). In the present study, even though glyoxylate shunt was considered in the reconstructed metabolic network, the simulated results indicated the absence of active glyoxylate shunt for both growth conditions which supports the increased flux through PEP-carboxylase. This is also in agreement with the previous report of a nonoperative glyoxylate shunt in the organism *C. protothecoides* obtained from ^{13}C flux analysis (Xiong et al. 2010).

In a photosynthetic organism, various anabolic reactions such as biosynthesis of lipids, chlorophyll, amino acids, and deoxy sugars are catalyzed by the NADPH dependent enzymes (Kanehisa et al. 2008). In order to satisfy this requirement of NADPH, NADH transhydrogenation reaction was found to be highly active under heterotrophic condition (Fig. 3a). However, reverse transhydrogenation reaction viz., NADPH to NADH was observed to be active (Fig. 2a) in case of photoautotrophic growth. Photophosphorylation and oxidative phosphorylation (Shastri and Morgan 2005) are the two key pathways that contribute toward cellular ATP generation for photoautotrophic growth. Further, functionality of oxidative phosphorylation is coupled with the utilization of NADH, the supply of which is satisfied by the high flux through reverse transhydrogenation reaction. Hence, oxidative phosphorylation was found to be active in both the cultivation conditions to fulfill the intracellular ATP requirements. Flux distribution in chlorophyll biosynthesis pathway was found to be 2.5-fold higher in case of photoautotrophic condition when compared to heterotrophic condition, which may be attributed toward harvesting of maximum amount of light

in the form of chemical energy (Fig. 4). Chlorophyll content of photoautotrophic biomass was observed to be 4-fold higher than heterotrophic biomass in case of *Chlorella vulgaris* (Fan et al. 2012).

The model predicted biomass yields for photoautotrophic and heterotrophic growths were 26.7 and 12.3 g mol^{-1} of carbon uptake, respectively. A similar observation of 1.6- and 1.9-fold increase in biomass yield per mole of carbon was reported for photoautotrophic growth of *Synechocystis* (Shastri and Morgan 2005) and *Chlamydomonas* (Boyle and Morgan 2009), respectively, when compared with the heterotrophic growth. The carbon efficiency (percentage of carbon flux fixed in biomass) of the heterotrophic condition was found to be 49.5 % which denotes that around 50.5 % of carbon is released as CO_2 during respiration of the cells (Navarro et al. 2009). Heterotrophic carbon uptake was ∼150 % higher (Fig. 4) than that of photoautotrophy which infers that more than half of the carbon consumed by the cell was used for energy production rather than biomass formation (Boyle and Morgan 2009).

Flux distribution during transition from nutrient sufficient phase to nutrient starvation phase of the growth of FC2

Over the time period of cultivation from 72 to 96 h, a shift in growth environment was observed in terms of transition from nutrient sufficient phase to the nutrient starvation phase, which was attributed to the exhaustion of phosphate as the rate limiting substrate under both heterotrophic and photoautotrophic conditions. Changes in intracellular flux distribution during this transition period were captured by performing FBA at 96 h of growth and compared with the flux values at 72 h. Model predicted specific growth rate and neutral lipid flux of the organism showed a reasonable match with the corresponding experimental values at 96 h of cultivation (Table 2). Flux estimates with two different objective functions M_μ and M_{NL} resulted in similar flux predictions, and no significant difference in the flux distributions were observed (Fig. 5a, b). Therefore, both the objective functions M_μ and M_{NL} were found suitable for flux analysis at 96 h of growth. The nutritional phase transition was marked with induction of neutral lipid accumulation in the biomass. For instance, at 96 h of growth carbon flux toward neutral lipid biosynthesis was found to be up regulated by 7-fold for M_μ (8-fold for M_{NL}) and 1.6-fold for M_μ (1.5-fold for M_{NL}) with respect to 72 h of photoautotrophic and heterotrophic cultivation, respectively (Fig. 5a, b). Under phosphate or nitrate starvation, the microalgae experiences a gradual decrease in growth rate, and the newly fixed carbon and chemical energy gets diverted toward neutral lipid accumulation which can generate more energy
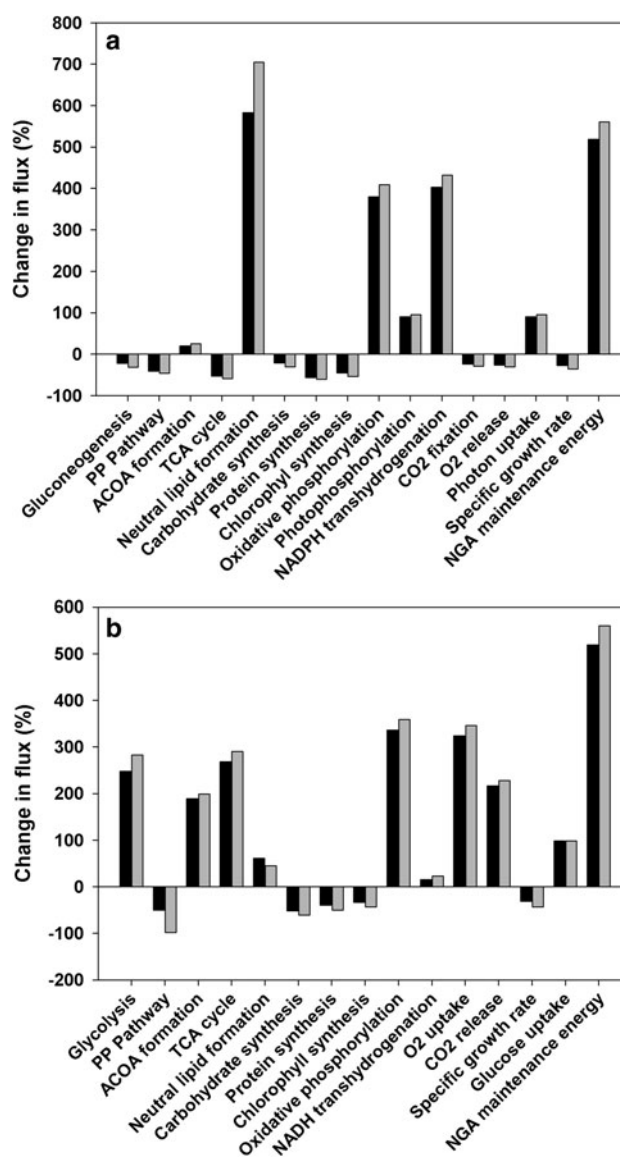

Fig. 5 Percentage change in absolute flux values at 96 h with respect to 72 h of growth under **a** photoautotrophic and **b** heterotrophic cultivation conditions. Black and gray bars indicate flux estimates at 96 h with the objective function *maximization of biomass* and *maximization of neutral lipids*, respectively. FBA at 72 h was performed considering *maximization of biomass* as the only objective function

upon oxidation than carbohydrates. Hence, the neutral lipids can serve as the best energy reserve for the cell under stress condition (Rodolfi et al. 2009).

An increased (∼6-fold for both M_μ and M_{NL}) NGA maintenance energy was observed at 96 h as compared to 72 h of growth under both cultivation conditions (Fig. 5a, b). This requirement of higher NGA maintenance energy in the nutritional starvation phase may be attributed to the various cellular maintenance operations under nutritional stress (Boyle and Morgan 2009). Our simulation results exhibited significantly elevated photon flux (2.5- to 2.75-fold)

Table 3 Balance for the cofactors NADPH, NADH, FADH$_2$ and ATP under photoautotrophic and heterotrophic conditions

Pathways	Photoautotrophic[a]			Heterotrophic[a]		
	M_μ 72[b]	M_μ 96[b]	M_{NL} 96[c]	M_μ 72[b]	M_μ 96[b]	M_{NL} 96[c]
NADPH balance						
Pentose phosphate	0.00	0.00	0.00	64.09	15.95	0.00
Calvin cycle	−217.63	−227.90	−231.29	–	–	–
Photophosphorylation	364.05	910.07	1000.91	–	–	–
Lipid synthesis	−11.81	−23.61	−26.97	−80.86	−53.44	−47.50
Nitrogen assimilation	−33.05	−20.24	−19.21	−90.31	−27.95	−22.89
Trans hydrogenation	−96.15	−634.92	−720.22	118.06	68.85	73.20
Other pathways	−5.35	−3.46	−3.22	−10.86	−3.40	−2.82
NADH balance						
Glycolysis and gluconeogenesis	18.38	19.78	21.18	148.25	186.29	190.88
ACOA and TCA cycle	12.25	16.06	17.63	354.70	627.46	661.27
Oxidative phosphorylation	−104.20	−656.91	−745.90	−325.82	−726.63	−763.99
Nitrogen assimilation	−11.02	−6.75	−6.40	−30.10	−9.32	−7.63
Trans hydrogenation	96.15	634.92	720.22	−118.06	−68.85	−73.20
Other pathways	−11.58	−7.13	−6.74	−28.93	−8.96	−7.34
FADH$_2$ balance						
TCA cycle	0.02	0.01	0.01	75.38	149.09	158.46
Oxidative phosphorylation	0.00	0.00	0.00	−75.03	−148.98	−158.37
Amino acid and protein	−0.03	−0.01	−0.01	−0.35	−0.11	−0.09
ATP balance						
Glycolysis and gluconeogenesis	45.68	44.96	47.47	149.25	187.12	191.49
ACOA and TCA cycle	0.02	0.01	0.01	75.38	149.09	158.46
Calvin cycle	−326.44	−341.84	−346.94	–	–	–
Photophosphorylation	467.80	1169.43	1286.17	–	–	–
Oxidative phosphorylation	260.49	1642.26	1864.74	927.11	2040.05	2147.52
Amino acid and protein	−30.35	−18.21	−17.26	−87.09	−26.83	−21.94
Maintenance energy	−291.98	−2371.66	−2713.18	−709.12	−2214.72	−2363.27
Biomass	−104.63	−99.31	−94.30	−285.38	−99.24	−81.17
Other pathways	−20.70	−25.81	−26.77	−70.38	−35.66	−31.16

[a] Cofactor balance obtained for energy yielding and consuming pathways under both heterotrophic and photoautotrophic conditions. The flux (mmol g^{-1} h^{-1}) values are expressed per 100 mmol CO$_2$ and 100 mmol glucose consumed for photoautotrophic and heterotrophic conditions respectively

[b] Cofactor balance obtained using *maximization of biomass* as objective function at 72 h (M_μ 72) and 96 h (M_μ 96)

[c] Cofactor balance obtained using *maximization of neutral lipid* as objective function at 96 h (M_{NL} 96)

toward generation of NADPH and ATP through photo-phosphorylation at 96 h time point as compared to 72 h of photoautotrophic cultivation to fulfill the required NGA maintenance energy (Table 3). In case of heterotrophic growth, the higher demand for NGA maintenance energy at 96 h time point was satisfied by the up regulated generation of NADH (1.6-fold), FADH$_2$ (2-fold), and ATP (1.5-fold) through glycolysis and TCA cycle (Table 3). Further, an increased oxidative phosphorylation flux at 96 h for both photoautotrophic and heterotrophic growths was also observed to generate required ATP from reducing equivalents. Interestingly, in spite of higher glucose and photon

uptake rates at 96 h of heterotrophic and photoautotrophic growth, respectively, a significant fraction of these was invested to meet high requirements of NGA maintenance energy under phosphate exhausted phase of the growth, and hence, biomass yield was observed to be reduced by 65 % which is in accordance with the previous report (Kliphuis et al. 2012).

In the present study, model predicted respiratory quotient (RQ) was found to be 1.47 (at 72 h) and 1.1 (at 96 h) for heterotrophic growth, and photosynthetic quotient (PQ) was found to be 1.29 (at 72 h) and 1.25 (at 96 h) in case of photoautotrophic growth. RQ and PQ values greater than
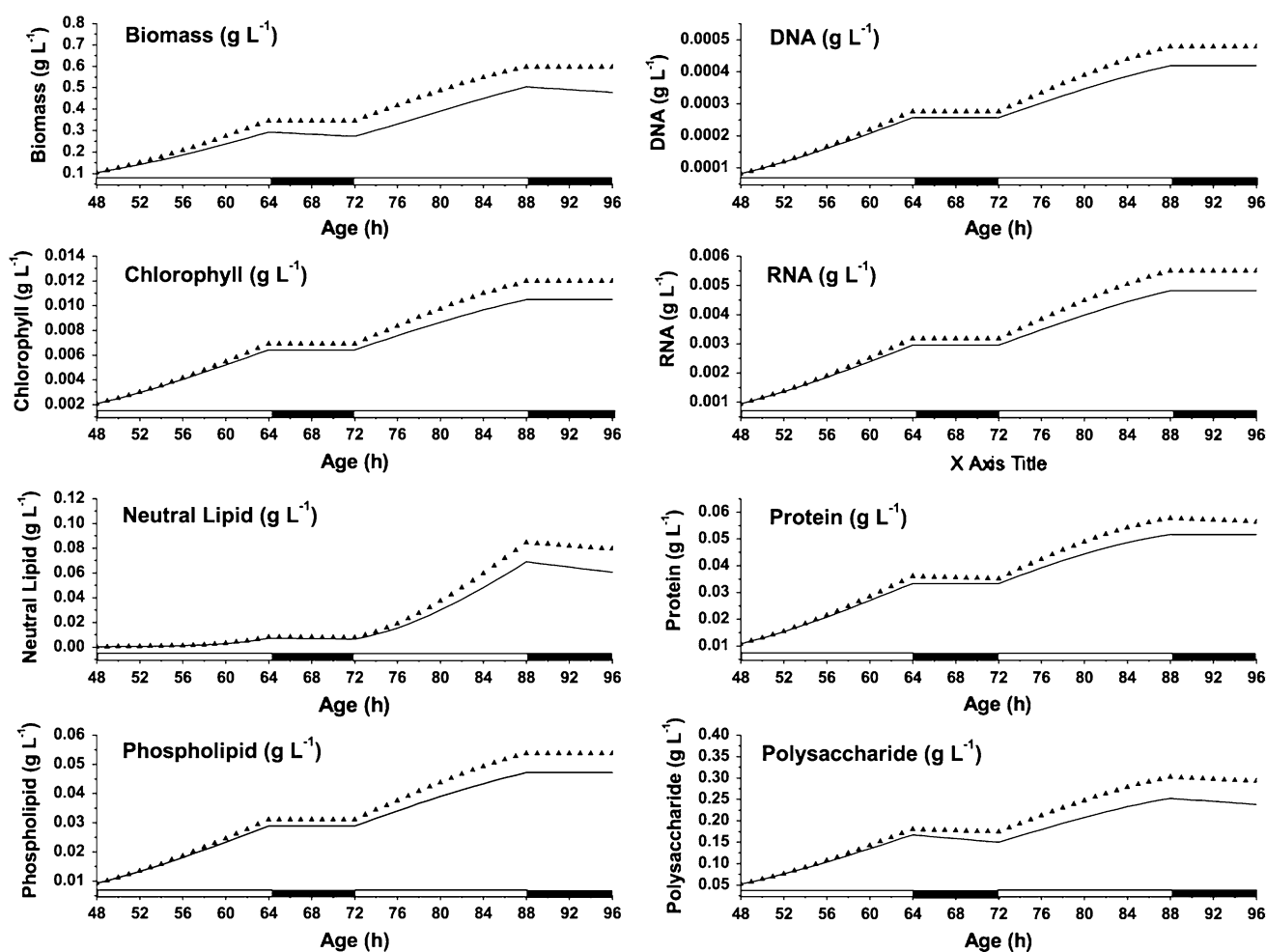
Fig. 6 Validation of dFBA via comparison of time evolution of intracellular biomass compositions predicted by the dynamic FBA (−) and kinetic model (···). The *white* and *black bars* on *X*-axis depicts 16 h light and 8 h dark cycle respectively over the time period of 48–96 h. The model predictions were obtained for the photoautotrophic growth of FC2 with a light intensity of 35 μmol photon m^{-2} s^{-1} and 16:8 light:dark cycle

one represent the presence of active lipid biosynthesis pathway in the organism (Barber and Blake 1985; Eriksen et al. 2007). Lipid is a highly reductive macromolecule of the cell and requires more NADPH for its biosynthesis. Hence, a fraction of NADPH pool was bifurcated from oxidative phosphorylation toward lipid biosynthesis resulting in decreased oxygen consumption and increased quotient values. Therefore, while a higher PQ and RQ were expected at 96 h, high requirement of NGA maintenance energy at this phase resulted in lower quotient values with respect to 72 h of growth.

dFBA for light–dark metabolism of FC2

Kinetic model and its validation

In the present study, two sets of experiments were used to estimate the kinetic parameters and model validation.

Initially, experimental data obtained by growing the culture at 20 μmol photons m^{-2} s^{-1} were used to estimate the kinetic parameters. Subsequently, the kinetic model was verified for photoautotrophic growth of the strain FC2 with a higher light intensity of 35 μmol photons m^{-2} s^{-1}. The purpose of the model validation was to test if the model was able to predict dynamic change in intracellular biomass composition associated with the light–dark cycle as captured by frequent experimental sampling.

The kinetic parameters of the model were estimated by fitting the simulated profile of biomass, substrates, and intracellular concentration of macromolecules with the corresponding experimental values (Fig. 1, Online Resource S2). The estimated model parameters are listed in Table 2 (Online Resource S2). Further, the kinetic model was experimentally validated for photoautotrophic growth of FC2 at a higher light intensity. A reasonably good fit was obtained for all the profiles as depicted by the R^2 values
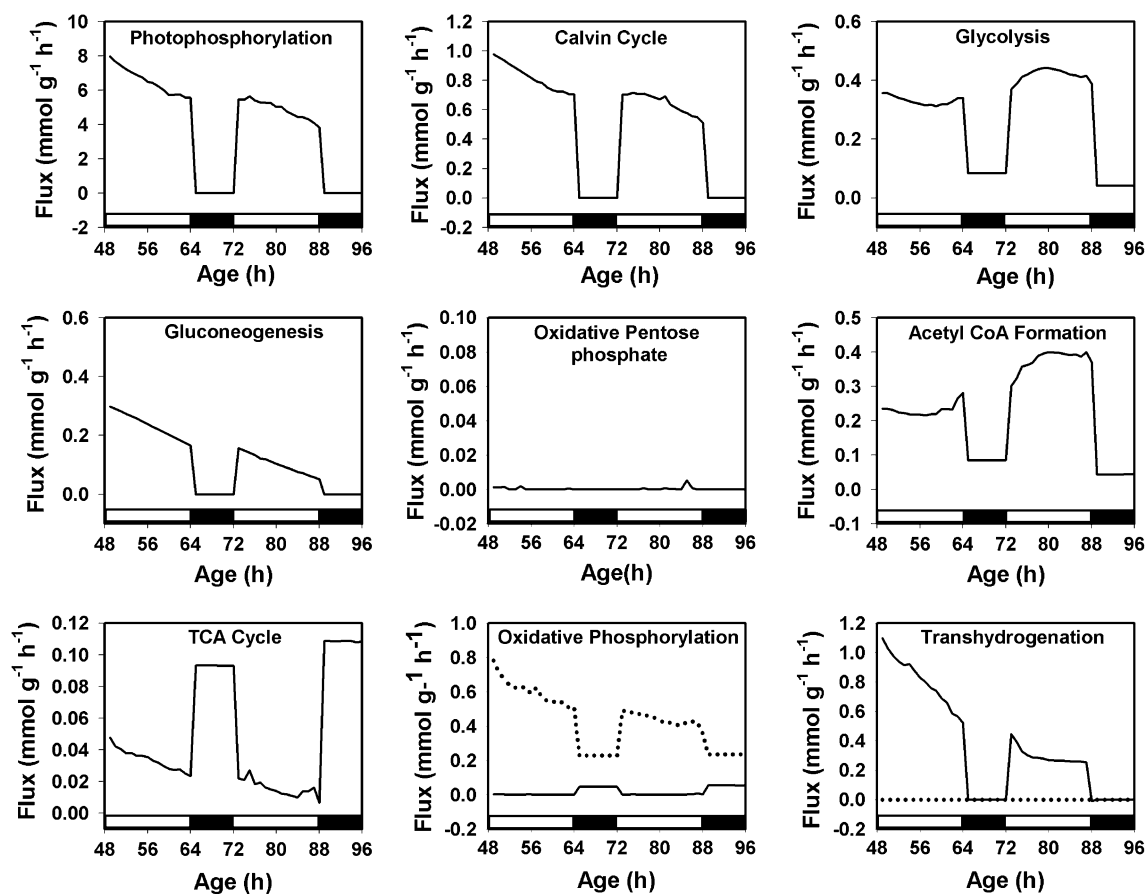
Fig. 7 Dynamic changes in the carbon flux distribution for light–dark metabolism of FC2. In case of oxidative phosphorylation, *dotted line* represents NADH dependent pathway and *solid line* represents FADH$_2$ dependent pathway. In case of transhydrogenation, *dotted line* represents NADH transhydrogenation and the *solid line* represents NADPH transhydrogenation. The *white* and *black bars* on X-axis depicts 16 h light and 8 h dark cycle, respectively, over the time period of 48–96 h. The flux values were obtained for the photoautotrophic growth of FC2 with a light intensity of 35 µmol photon m^{-2} s^{-1} and 16:8 light:dark cycle. All the flux values were expressed in mmol g^{-1} DCW h^{-1}

ranging in between 0.90 and 0.95 (Fig. 2, Online Resource S2). While, the dynamic substrate (nitrate, CO$_2$, and light intensity) utilization rates predicted by kinetic model were used as inputs for dFBA analysis, the time evolution of intracellular composition was used for validation of dFBA simulation.

Dynamic FBA

The dynamic macromolecular concentration of biomass was obtained by carrying out FBA over each pseudo steady state time interval followed by integration over the interval. These dynamic macromolecular concentrations obtained from dFBA were validated by comparing with the corresponding profiles predicted by the kinetic model. The dFBA predictions for biomass, protein, carbohydrate, neutral lipid, polar lipid, chlorophyll, DNA, and RNA were found to be in agreement with the corresponding kinetic profiles (Fig. 6). This point toward reliability of flux estimates obtained from dFBA.

Flux toward photophosphorylation was high in the light phase of the metabolism, and a complete shut off was predicted as soon as the cell entered into the dark phase (Fig. 7). A reverse trend was observed in case of TCA cycle flux which was minimally operating in the light phase followed by significant up regulation in the dark cycle. While the active photophosphorylation in the light cycle was to satisfy the GA and NGA maintenance energy requirements, the role of TCA cycle was mainly to provide the precursors for protein biosynthesis. The elevated TCA cycle in the dark metabolism was responsible for supplying NGA maintenance energy. A similar up regulation in TCA cycle mRNA pool was reported for dark metabolism of *Synechocystis* sp. as compared to light cycle (Knoop et al. 2013). As the photophosphorylation was sufficient to fulfill the requirement of reducing equivalent, oxidative PP was inactive in photoautotrophic growth. Calvin cycle, oxidative phosphorylation, NADPH transhydrogenation reaction, and photophosphorylation are highly interdependent

pathways under photoautotrophic growth, and hence, similar flux profile was observed in all these pathways. Matching flux profiles for Calvin cycle and photophosphorylation were also predicted via dFBA of *Synechocystis* sp. under light–dark cycle (Knoop et al. 2013). The glycolytic and ACOA flux remained constant over the light period of 48–64 h. However, in the subsequent light phase of 72–88 h a steady increase in carbon flux was predicted for both glycolytic and ACOA nodes (Fig. 7). In the present study, neutral lipid accumulation was induced only at ∼72 h of photoautotrophic growth (Fig. 1 in Online Resource S2). Hence, this gradual increase in glycolytic flux may be attributed toward requirement of ACOA as a precursor for neutral lipid biosynthesis. Glycolysis and ACOA formation were found to be down regulated when cellular metabolism entered into the dark phase. Redirection of carbon flux from polysaccharide and neutral lipid (Fig. 3, Online Resource S2) resulted in increased TCA cycle and nonzero ACOA flux in the dark phase of the growth. dFBA in *Synechocystis* sp. showed glycogen degradation during the dark cycle of diurnal growth which is in accordance with the present finding (Knoop et al. 2013). Carbon flux in gluconeogenesis and in turn polysaccharide biosynthesis was maximum in the beginning of the light phase followed by gradual decrease which was concomitant with the decrease in specific growth rate over the cultivation period. It is important to note that, unlike static FBA, dFBA predicted an unaltered NGA of 1.5 mmol g^{-1} DCW h^{-1}.

References

Barber BJ, Blake NJ (1985) Substrate catabolism related to reproduction in the bay scallop *Argopecten irradians concentricus*, as determined by O/N and RQ physiological indexes. Mar Biol 87:13–18

Barsanti L, Gualtieri P (2006) Algae: anatomy, biochemistry, and biotechnology. Taylor & Francis, New York

Boyle NR, Morgan JA (2009) Flux balance analysis of primary metabolism in *Chlamydomonas reinhardtii*. BMC Syst Biol 3(4):1–14

Cataldo DA, Maroon M, Schrader LE, Youngs VL (1975) Rapid colorimetric determination of nitrate in plant tissues by nitration of salicylic acid. Commun Soil Sci Plant Anal 6:71–80

Chen W, Zhang C, Song L, Sommerfeld M, Hu Q (2009) A high throughput Nile red method for quantitative measurement of neutral lipids in microalgae. J Microbiol Methods 77:41–47

DalMolin CGO, Quek LE, Palfreyman RW, Nielsen LK (2011) AlgaGEM- a genome-scale metabolic reconstruction of algae based on the *Chlamydomonas reinhardtii* genome. BMC Genomics 12(4):1–10

Dormann P, Benning C (2002) Galactolipids rule in seed plants. Trends Plant Sci 7(3):112–118

El-sheekh MM (1993) Lipid and fatty acids composition of photoautotrophically and heterotrophically grown *Chlamdomonas reinhardtii*. Biol Plantarum 35(3):435–441

Eriksen NT, Riisgard FK, Gunther WS, Iversen JJL (2007) On-line estimation of O_2 production, CO_2 uptake, and growth kinetics of microalgal cultures in a gas-tight photobioreactor. J Appl Phycol 19(2):161–174

Fan J, Huang J, Li Y et al (2012) Sequential heterotrophy-dilution–photoinduction cultivation for efficient microalgal biomass and lipid production. Bioresour Technol 112:206–211

Fuentes MMR, Fernandez GGA, Perez JAS, Guerrero JLG (2000) Biomass nutrient profiles of the microalga *Porphyridium cruentum*. Food Chem 70(3):345–353

Hu Q, Sommerfeld M, Jarvis E et al (2008) Microalgal triacylglycerols as feedstocks for biofuel production: perspectives and advances. Plant J 54:621–639

Kanehisa M, Araki M, Goto S et al (2008) KEGG for linking genomes to life and the environment. Nucleic Acids Res 36:D480–D484

Kleessen S, Nikoloski Z (2012) Dynamic regulatory on/off minimization for biological systems under internal temporal perturbations. BMC Syst Biol 6(16):1–13

Kliphuis AMJ, Klok AJ, Martens DE, Lamers PP, Janssen M, Wijffels RH (2012) Metabolic modelling of *Chlamydomonas reinhardtii*: energy requirements for photoautotrophic growth and maintenance. J Appl Phycol 24(2):253–266

Knoop H, Gründel M, Zilliges Y, Lehmann R, Hoffmann S, Lockau W, Steuer R (2013) Flux balance analysis of Cyanobacterial metabolism: the metabolic network of *Synechocystis* sp. PCC6803. PLoS Comput Biol 9(6):1–15

Lim DKY, Garg S, Timmins M, Zhang ESB, Thomas-Hall SR, Schuhmann H, Li Y, Schenk PM (2012) Isolation and evaluation of oil-producing microalgae from subtrophical coastal and brackish waters. PLoS ONE 7(7):e40751. doi:10.1371/journal.pone.0040751

Mahadevan R, Edwards JS, Dyle FJ (2002) Dynamic flux balance analysis of diauxic growth in *Escherichia coli*. Biophys J 83:1331–1340

Montagud A, Navarro E, Cordoba PF, Urchueguia JF, Patil KR (2010) Reconstruction and analysis of genome-scale metabolic model of a photosynthetic bacterium. BMC Syst Biol 4(156):1–16

Navarro E, Montagud A, Fernández de Córdoba P, Urchueguía JF (2009) Metabolic flux analysis of the hydrogen production potential in *Synechocystis* sp. PCC6803. Int J Hydrogen Energy 34:8828–8838

Parsons TR, Maita Y, Lalli CM (1984) A manual of chemical and biological methods for seawater analysis, 1st edn. Pergamon Press Ltd, Great Britain

Pruvost J, Van Vooren G, Le Gouic B, Couzinet-Mossion A, Legrand J (2011) Systematic investigation of biomass and lipid productivity by microalgae in photobioreactors for biodiesel application. Bioresour Technol 102:150–158

Rodolfi L, Zittelli GC, Bassi N, Padovani G, Biondi N, Bonini G, Tredici MR (2009) Microalgae for oil: strain selection, induction of lipid synthesis and outdoor mass cultivation in a low-cost photobioreactor. Biotechnol Bioeng 102(1):100–112

Shastri AA, Morgan JA (2005) Flux balance analysis of photoautotrophic metabolism. Biotechnol Prog 21:1617–1626

Srivastava RK, Maiti SK, Das D, Bapat PM, Batta K, Bhushan M, Wangikar PP (2012) Metabolic flexibility of D-ribose producer strain of *Bacillus pumilis* under environmental perturbations. J Ind Microbiol Biotechnol 39:1227–1243

Varma A, Palsson BO (1994) Stoichiometric flux balance models quantitatively predict growth and metabolic by-product secretion in wild-type *Escherichia coli* W3110. Appl Environ Microbiol 60:3724–3731

Xiong W, Liu L, Wu C, Yang C, Wu Q (2010) ^{13}C-tracer and gas chromatography–mass spectrometry analysis reveal metabolic flux distribution in the oleaginous microalga *Chlorella protothecoides*. Plant Physiol 154:1001–1011

Yang C, Hua Q, Shimizu K (2000) Energetics and carbon metabolism during growth of microalgal cells under photoautotrophic, mixotrophic and cyclic light-autotrophic/dark-heterotrophic conditions. Biochem Eng J 6(2):87–102

Yugi K, Nakayama Y, Kinoshita A, Tomita M (2005) Hybrid dynamic/static method for large-scale simulation of metabolism. Theor Biol Med Model 2(42):1–11